INTERNATIONAL JOURNAL FOR NUMERICAL METHODS IN ENGINEERING
Int. J. Numer. Meth. Engng 2007; **69**:1278–1304
Published online 31 July 2006 in Wiley InterScience (www.interscience.wiley.com). DOI: 10.1002/nme.1808

Optimal layout design of three-dimensional geometrically non-linear structures using the element connectivity parameterization method

Gil Ho Yoon[‡], Young Soo Joung[§] and Yoon Young Kim[*,†]

National Creative Research Initiatives Center for Multiscale Design and School of Mechanical and Aerospace Engineering, Seoul National University, Kwanak-Gu, Shinlim-Dong San 56-1, Seoul 151-742, Korea

SUMMARY

The topology design optimization of 'three-dimensional geometrically-non-linear' continuum structures is still difficult not only because of the size of the problem but also because of the unstable continuum finite elements that arise during the optimization. To overcome these difficulties, the element connectivity parameterization (ECP) method with two implementation formulations is proposed. In ECP, structural layouts are represented by inter-element connectivity, which is controlled by the stiffness of element-connecting zero-length links. Depending on the link location, ECP may be classified as an external ECP (E-ECP) or an internal ECP (I-ECP). In this paper, I-ECP is newly developed to substantially enhance computational efficiency. The main idea in I-ECP is to reduce system matrix size by eliminating some internal degrees of freedom associated with the links at voxel level. As for ECP implementation with commercial software, E-ECP, developed earlier for two-dimensional problems, is easier to use even for three-dimensional problems because it requires only numerical analysis results for design sensitivity calculation. The characteristics of the I-ECP and E-ECP methods are compared, and these methods are validated with numerical examples. Copyright © 2006 John Wiley & Sons, Ltd.

Received 26 August 2005; Revised 30 April 2006; Accepted 15 May 2006

KEY WORDS: topology optimization; three-dimensional structures; element connectivity parameterization

*Correspondence to: Yoon Young Kim, School of Mechanical and Aerospace Engineering, Seoul National University, Kwanak-Gu San 56-1, Seoul 151-742, Korea.
†E-mail: yykim@snu.ac.kr
‡E-mail: ghy@mek.dtu.dk
§E-mail: ys188@idealab.snu.ac.kr

Contract/grant sponsor: Korea Science Foundation

1. INTRODUCTION

In this investigation, two objectives are pursued: (i) the expansion of the existing version of the element connectivity parameterization (ECP method) for the topology optimization of three-dimensional continuum bodies exhibiting geometrical non-linearity [1, 2] and (ii) the development of a new computationally-efficient version of the ECP method. Even with the maturity of the density-based topology optimization methods using the Solid Isotropic Material with Penalization (SIMP) scheme, the topology optimization of geometrically non-linear structures is still a challenging problem because of the numerical instability in low-density regions [3, 4].

Figure 1 shows some examples where unstable elements appear in two- and three-dimensional structures. The density-based SIMP method varies element densities to define desired topological layouts. Thus, low-density elements may become inverted and have negative volumes or areas under large displacements. These phenomena are responsible for poor convergence or divergence in numerical analysis. Although some density-based methods were suggested [5–9] to overcome these difficulties, they still encountered difficulties especially for three-dimensional geometrically non-linear structures; the topology optimization of such structures has been seldom considered [3, 10, 11]. Both numerical stability and computational efficiency are required to optimize these structures successfully. Therefore, a new ECP approach to fulfill these two criteria is proposed in this study. Also, the expansion of the existing ECP method mainly developed for two-dimensional problems to three-dimensional problems will be also discussed because it can be implemented on commercial software.

1.1. Element connectivity parameterization method

The element connectivity parameterization (ECP) method has been recently proposed to resolve the numerical instability in two-dimensional problems [1]. Unlike popular density-based approaches,

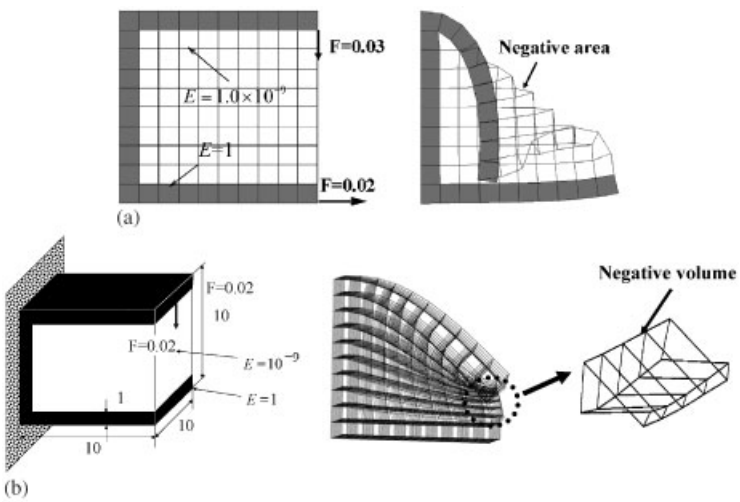

Figure 1. Examples of unstable elements under large displacement: (a) the two-dimensional case; and (b) the three-dimensional case.

DOI: 10.1002/nme

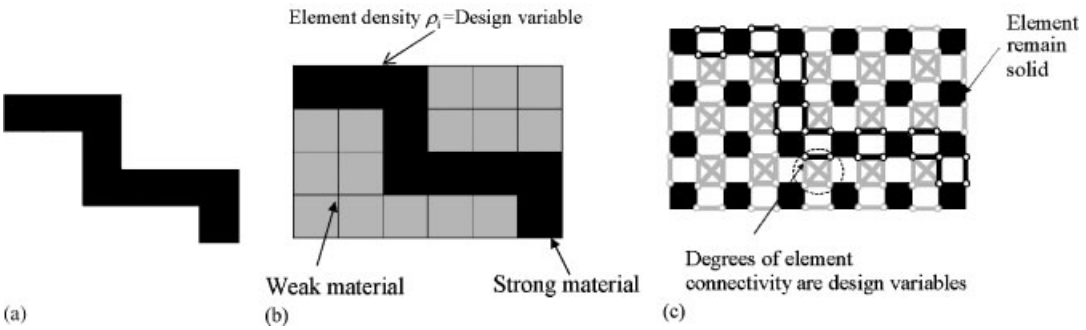

Figure 2. Modelling comparison: (a) a given topological layout; (b) modelling by the element density method; and (c) modelling by the element connectivity parameterization method.

the ECP method represents structural layouts by the degrees of the inter-element connectivity controlled by the stiffness of the zero-length elastic links connecting inter-element nodes, and not by the element density-dependent stiffness. Since the discretizing finite elements hold the original material properties throughout the optimization process, no numerical problem related to low-density elements occurs. It is interesting to note some similarity between the present ECP approach and the discontinuous Galerkin method (see, e.g. Reference [12]). The discontinuous Galerkin method is not developed to treat the low-density element problem discussed above, but both the discontinuous Galerkin method and the ECP method allow element interfacial discontinuity.[¶]

To compare the main difference between the ECP method and the element density method, let us consider a layout in Figure 2(a). Figure 2(b) shows the model used by the density method to represent the layout in Figure 2(a) while Figure 2(c) shows the model used by the ECP method. Because plane or volume elements in the ECP method [1, 2] remain solid and a topology is defined by a distribution of the stiffness of zero-length links, the unstable phenomena caused by weak elements cannot occur.

In spite of the apparent advantage of the ECP method in numerical stability, the model shown in Figure 2(c) requires more nodes and consequently, more computation time. Thus, the ECP modelling increases the matrix size by four times and by eight times than in the element density based approaches for two-dimensional cases and three-dimensional cases, respectively; the computation time increase resulting from the increase system size especially for three-dimensional problems may not be overlooked. However, the existing ECP method developed in References [1, 2] can be directly implemented by using any commercial software such as ANSYS. In the ECP implementation of References [1, 2], the analytic sensitivity for the end compliance can be obtained without having a computer source code.

A new version of the ECP method that does not increase the system matrix size is also developed in this investigation. This new version, called the internal ECP method (in short, I-ECP method), is very useful in dealing with three-dimensional problems requiring a large amount of computation. The key idea of the I-ECP method is the static condensation of some degrees of freedom at pixel

[¶]During the revision, the penalty method for topology optimization [13] utilizing the discontinuous Galerkin formulation is brought to our attention. In Reference [13], the relation between the penalty method and the ECP method is also briefly remarked.

DOI: 10.1002/nme

(or voxel) level. To distinguish I-ECP from the existing ECP method, the existing ECP method in Reference [1] will be called the external-ECP (E-ECP). Unlike the E-ECP method connecting solid elements by external links, the I-ECP assumes that each element is supported by internal links. The detailed characteristics of I-ECP and E-ECP will be explained and compared in the Section 2.

2. EXTERNAL AND INTERNAL ECP FORMULATION

2.1. Field equation for geometrically non-linear analysis

In this section, equations needed for topology optimization formulation of three-dimensional geometrically non-linear structures will be briefly given. To consider geometrically non-linear effects, the Green–Lagrangian strain (${}^{t+\Delta t}_{0}\varepsilon_{ij}$) and the second Piola–Kirchoff stress (${}^{t+\Delta t}_{0}S_{ij}$) will be used. All notations given in this section are based on Bathe [14]. The position and the displacement of a generic point in a body at time t are denoted by ${}^{t}x_i$ and ${}^{t}u_i$, respectively. The incremental form of position and displacement can be written as (1) where the updated displacement from time t to $t+\Delta t$ is denoted by u_i

$$ {}^{t}x_i = {}^{0}x_i + {}^{t}u_i, \quad {}^{t+\Delta t}u_i = {}^{t}u_i + u_i \quad (i=1,2,3) \tag{1} $$

The Green–Lagrangian strain ${}^{t+\Delta t}_{0}\varepsilon_{ij}$ is defined as

$$ {}^{t+\Delta t}_{0}\varepsilon_{ij} = \frac{1}{2}\left(\frac{\partial^{t+\Delta t}u_i}{\partial^{0}x_j} + \frac{\partial^{t+\Delta t}u_j}{\partial^{0}x_i} + \frac{\partial^{t+\Delta t}u_k}{\partial^{0}x_i}\frac{\partial^{t+\Delta t}u_k}{\partial^{0}x_j} \right) \tag{2} $$

The following linear constitutive equation relating ${}^{t+\Delta t}_{0}\varepsilon_{ij}$ and ${}^{t+\Delta t}_{0}S_{ij}$ at time $t+\Delta t$ will be used:

$$ {}^{t+\Delta t}_{0}S_{ij} = C_{ijkl}\,{}^{t+\Delta t}_{0}\varepsilon_{kl} \tag{3} $$

where the matrix form of C_{ijkl} may be written as

$$ \mathbf{C} = \frac{E(1-v)}{(1+v)(1-2v)} \begin{bmatrix} 1 & \frac{v}{1-v} & \frac{v}{1-v} & 0 & 0 & 0 \\ \frac{v}{1-v} & 1 & \frac{v}{1-v} & 0 & 0 & 0 \\ \frac{v}{1-v} & \frac{v}{1-v} & 1 & 0 & 0 & 0 \\ 0 & 0 & 0 & \frac{1-2v}{2(1-v)} & 0 & 0 \\ 0 & 0 & 0 & 0 & \frac{1-2v}{2(1-v)} & 0 \\ 0 & 0 & 0 & 0 & 0 & \frac{1-2v}{2(1-v)} \end{bmatrix} \tag{4} $$

In Equation (4), E and v are Young's modulus and Poisson's ratio, respectively [14].

DOI: 10.1002/nme

It is convenient to decompose the strain increment ${}_0\varepsilon_{ij}$ into the linear term, ${}_0e_{ij}$ and the non-linear term, ${}_0\eta_{ij}$ as

$$ {}^{t+\Delta t}_{0}\varepsilon_{ij} = {}^{t}_{0}\varepsilon_{ij} + {}_0\varepsilon_{ij}, \quad {}_0\varepsilon_{ij} = {}_0e_{ij} + {}_0\eta_{ij} \tag{5} $$

$$ {}_0\eta_{ij} = \tfrac{1}{2}({}^{t}_{0}u_{k,i}\,{}_0u_{k,j}) \tag{6} $$

$$ {}_0e_{ij} = \tfrac{1}{2}({}_0u_{i,j} + {}_0u_{j,i} + {}^{t}_{0}u_{k,i}\,{}_0u_{k,j} + {}_0u_{k,i}\,{}^{t}_{0}u_{k,j}) \tag{7} $$

In terms of ${}_0e_{ij}$ and ${}_0\eta_{ij}$, the linearized principle of virtual work for the initial analysis domain ${}^0V$ can be written as

$$ \int_{{}_0V} C_{ijrs}\,{}_0e_{rs}\delta\,{}_0e_{ij}\,\mathrm{d}\,{}^0V + \int_{{}_0V} {}^{t}_{0}S_{ij}\delta\,{}_0\eta_{ij}\,\mathrm{d}\,{}^0V = {}^{t+\Delta t}R - \int_{{}_0V} {}^{t}_{0}S_{ij}\delta\,{}_0e_{ij}\,\mathrm{d}\,{}^0V \tag{8} $$

where the external force is denoted by ${}^{t+\Delta t}R$. After applying the standard finite element procedure to Equation (8), a matrix equation representing the equilibrium can be derived. For numerical analysis of the resulting equation, the standard Newton–Raphson procedure is used. The incremental equations needed to solve the geometrically non-linear problem are as follows [12]:

$$ {}^{t+\Delta t}\mathbf{U}^{(k)} = {}^{t+\Delta t}\mathbf{U}^{(k-1)} + \Delta\mathbf{U}^{(k)}, \quad {}^{t+\Delta t}\mathbf{U}^{(0)} = {}^{t}\mathbf{U} \tag{9} $$

$$ \underbrace{\Re({}^{t+\Delta t}\mathbf{U}^{(k-1)})}_{\text{Residual Force}} = \underbrace{({}^{t}\mathbf{K}_{\mathrm{T}}^{(k-1)})}_{\text{Tangent stiffness matrix}} \Delta\mathbf{U}^{(k)} = \underbrace{{}^{t+\Delta t}\mathbf{R}}_{\text{External Force}} - \underbrace{{}^{t+\Delta t}_{0}\mathbf{F}^{(k-1)}}_{\text{Internal Force}} \tag{10} $$

where ${}^{t}\mathbf{K}_{\mathrm{T}}^{(k-1)}$ and ${}^{t+\Delta t}_{0}\mathbf{F}^{(k-1)}$ are the tangent stiffness matrix of plane or solid elements at time t of iteration $(k-1)$ and the internal force vector at time $t+\Delta t$ of iteration $(k-1)$, respectively. The displacement vector is denoted by ${}^{t+\Delta t}\mathbf{U}^{(k)}$. The symbol ${}^{t+\Delta t}\mathbf{R}$ denotes the applied force vector at time $t+\Delta t$. See Bathe [14] for detailed expressions of ${}^{t}\mathbf{K}_{\mathrm{T}}^{(k-1)}$, etc.

2.2. External ECP

First, we will present how the existing E-ECP method developed for two-dimensional problems can be extended to three-dimensional problems. The issues in the extension are how to define links suitable for three-dimensional problems and how to construct a finite element model connected by the links suitable for topology optimization (by using commercial finite element software). Figure 3 shows the suggested link modelling technique for three-dimensional structures discretized by solid elements. The number of links will depend on the number of the solid elements interfacing the same node. Link connectivity is illustrated in Figure 3(a), where 'Connection' stands for the location where nodes of adjacent solid elements are connected. (A connection would be a global node in the standard finite element modelling.) A typical three-dimensional layout represented by strong and weak links (having high and low stiffness values, respectively) is illustrated in Figure 3(b). Since solid elements are connected by external links, this ECP method will be called the external ECP, in short, E-ECP. (The meaning of 'external' will be clear when the internal ECP method is presented later.)

DOI: 10.1002/nme

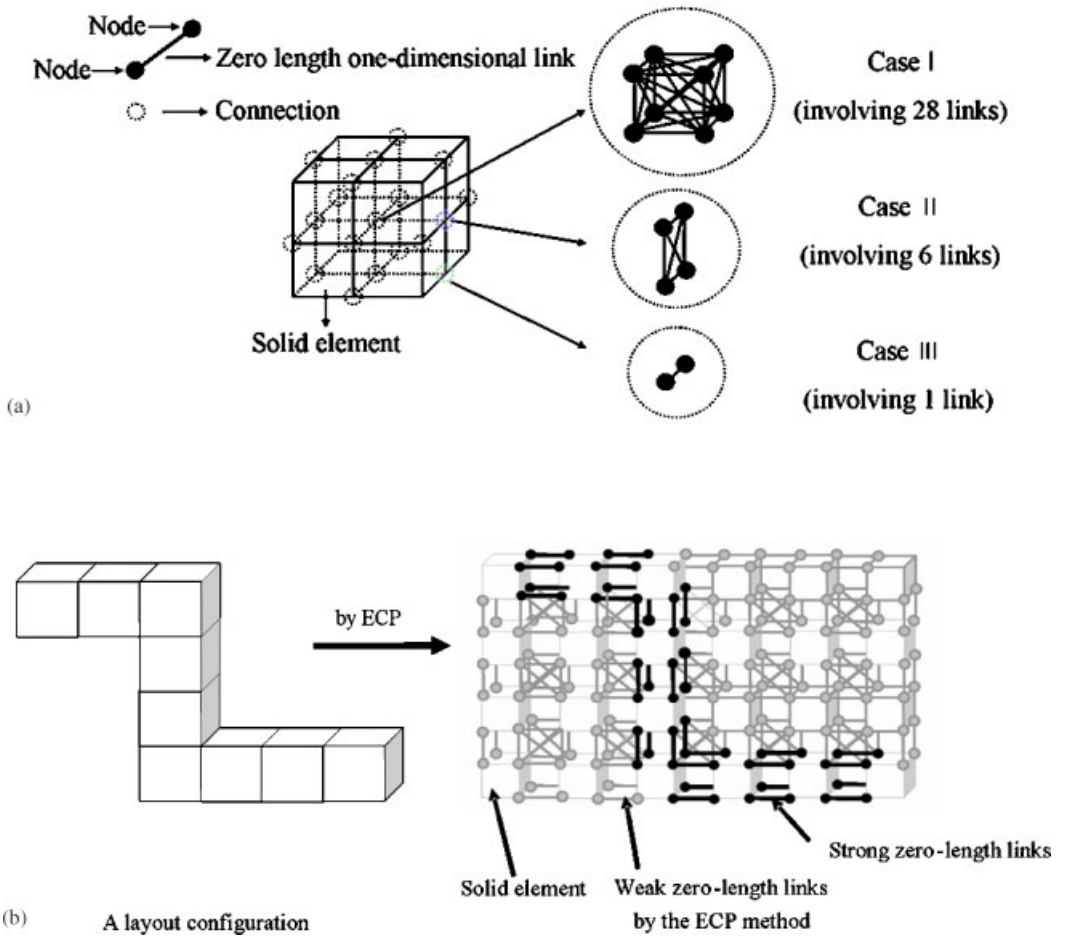

Figure 3. The modelling technique of the E-ECP method applied to three-dimensional structures: (a) illustration of solid elements connected by 'zero-length' links (The link stiffness controls the degree of the inter-element connectivity.); and (b) a modelling example by the E-ECP method.

For the topology optimization of three-dimensional bodies, the link is assumed to have varying stiffness in all of the three spatial directions. Thus, the stiffness matrix of an eth link connecting nodes p and q shown in Figure 4 is defined as

$$k_e^{\text{link}} = l_e k_{\text{nominal}}^{\text{link}} \tag{11}$$

where k_e^{link} and l_e are the stiffness matrix of an eth link and its stiffness value, respectively. In the E-ECP method, l_e is parameterized as a function of the design variable γ_e that is assigned to every link. Because the link is a one-dimensional element, the nominal dimensionless stiffness matrix

DOI: 10.1002/nme

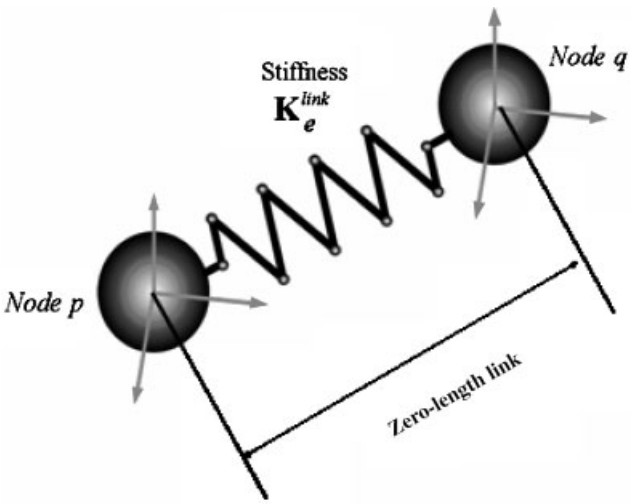

Figure 4. An eth link connecting node p and q defined in the three-dimensional spatial space.

$k_{\text{nominal}}^{\text{link}}$ can be written as

$$k_{\text{nominal}}^{\text{link}} = \begin{bmatrix} 1 & 0 & 0 & -1 & 0 & 0 \\ 0 & 1 & 0 & 0 & -1 & 0 \\ 0 & 0 & 1 & 0 & 0 & -1 \\ -1 & 0 & 0 & 1 & 0 & 0 \\ 0 & -1 & 0 & 0 & 1 & 0 \\ 0 & 0 & -1 & 0 & 0 & 1 \end{bmatrix} \tag{12}$$

The stiffness value l_e can be parameterized by various functions but the following function, similar to the RAMP interpolation function (see, e.g. Reference [4]), is selected in this work:

$$l_e = \alpha \frac{\gamma_e^n}{1 + (1 - \gamma_e^n) \times m} + \beta \tag{13a}$$

$$\alpha = l_{\max} - l_{\min}, \quad \beta = l_{\min} \tag{13b}$$

$$0 = \gamma_{\text{LOW}} \leqslant \gamma_e \leqslant \gamma_{\text{UPPER}} = 1 \tag{14}$$

In Equation (13), $l_{\max}$ and $l_{\min}$ are the upper bound and the lower bound of the link stiffness, respectively, and n and m are penalization factors. Based on the findings of earlier studies [1, 2, 15], $l_{\max}$ is set to be $O(10^4 \times k_{\text{diagonal}})$ where k_{diagonal} denotes the diagonal term of the stiffness matrices of adjacent elements. The value of $l_{\min}$ is chosen to be $O(10^{-9} \times k_{\text{diagonal}})$. When γ_e approaches either γ_{LOW} or γ_{UPPER}, the nodes connected by the eth link can be regarded to be connected or disconnected.

DOI: 10.1002/nme

The topology optimization dealing with three-dimensional non-linear problems tends to yield more local optima than the optimization dealing with two-dimensional problems. For instance, out-of-plane buckling, non-existent in two-dimensional problems, can take place during optimization, so unsymmetric layouts even under symmetric conditions may be obtained. To obtain stable close-to-global optimal solutions, several strategies were tested. Among them, the continuation method [6] that increases penalization factors over a few optimization stages was effective. In the present numerical problems, lower factors of n between 1 and 3, and m between 0 and 3 were used for the first optimization stage. Then, the values of the factors were increased and the optimization processes were repeated.

To explain the ECP method, we begin with the well-known linearized equilibrium equation for three-dimensional problems (the detailed procedure may be found in Reference [1])

$$\underbrace{({}^{t}\mathbf{K}_{\mathrm{T}}^{(k-1)})}_{\substack{\text{Tangent stiffness}\\ \text{of the external ECP}}} \Delta\mathbf{U}^{(k)} = \underbrace{\Re^{(k-1)}}_{\text{Residual Force}} \tag{15}$$

$${}^{t+\Delta t}\mathbf{U}^{(k)} = {}^{t+\Delta t}\mathbf{U}^{(k-1)} + \Delta\mathbf{U}^{(k)} \tag{16}$$

$$\underbrace{\Re^{(k-1)}}_{\text{Residual Force}} = \underbrace{{}^{t+\Delta t}\mathbf{R}}_{\text{External Force}} - \underbrace{{}^{t+\Delta t}_{0}\mathbf{F}^{\text{structure},(k-1)}}_{\substack{\text{Internal force from}\\ \text{the discretizing elements}}} - \underbrace{{}^{t+\Delta t}_{0}\mathbf{F}^{\text{link},(k-1)}}_{\substack{\text{Internal force from}\\ \text{the zero-length links}}} \tag{17}$$

$${}^{t}\mathbf{K}_{\mathrm{T}}^{(k-1)} = {}^{t}\mathbf{K}_{\mathrm{T}}^{\text{structure},(k-1)} + \mathbf{K}^{\text{link}}(\boldsymbol{\gamma}) \tag{18}$$

$${}^{t}\mathbf{K}_{\mathrm{T}}^{\text{structure},(k-1)} = \sum_{i=1}^{N_p} {}^{t}k_{\mathrm{T},i}^{\text{structure},(k-1)}$$

$${}^{t+\Delta t}_{0}\mathbf{F}^{\text{structure},(k-1)} = \sum_{i=1}^{N_p} {}^{t+\Delta t}_{0}f_{i}^{\text{structure},(k-1)} \tag{19}$$

In Equations (15)–(19), ${}^{t}\mathbf{K}_{\mathrm{T}}^{(k-1)}$, ${}^{t+\Delta t}\mathbf{R}$, and $\Re^{(k-1)}$ denote the tangent stiffness matrix, the external force, and the residual force vector at the $(k-1)$th iteration, respectively. The symbols N_p and N_e denote the number of the discretizing solid elements and the number of zero-length links, respectively. The quantities defined at the element level are represented by small letters such as ${}^{t}k_{\mathrm{T},i}^{\text{structure},(k-1)}$.

The definitions of $\mathbf{K}^{\text{link}}(\boldsymbol{\gamma})$ and ${}^{t+\Delta t}_{0}\mathbf{F}^{\text{link},(k-1)}$ are

$$\mathbf{K}^{\text{link}}(\boldsymbol{\gamma}) = \sum_{i=1}^{N_e} k_i^{\text{link}}(\gamma_i) \tag{20}$$

$${}^{t+\Delta t}_{0}\mathbf{F}^{\text{link},(k-1)} = \sum_{i=1}^{N_e} [k_i^{\text{link}} \times {}^{t+\Delta t}u_i^{(k-1)}] \tag{21}$$

As shown in Figure 3(a), the most general connection case, Case I, has 28 links that connect eight adjacent solid elements. However, only one design variable γ_i will be introduced to each

DOI: 10.1002/nme

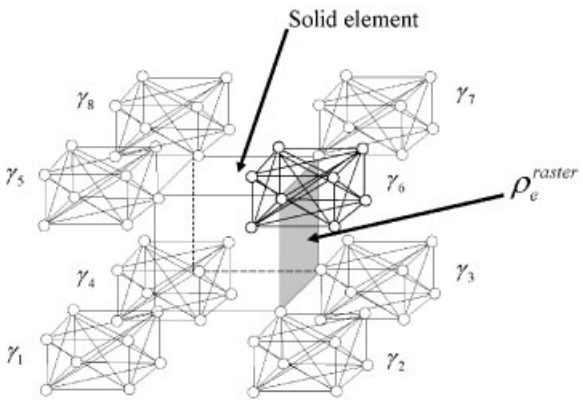

Figure 5. A three-dimensional element surrounded by a set of zero-length link elements.

connection; therefore, the stiffnesses of all 28 links for Case I and 6 links for Case II and stiffness of 1 link for Case III are controlled by a single design variable.

To represent the optimal structural layout from the optimized distribution of the link design variables, the raster imaging scheme is used. This scheme calculates the density of a solid element, ρ_e^{raster} as the average of the design variables of all links surrounding the element. For example, the density of an eth solid element shown in Figure 5 is

$$\rho_e^{\text{raster}} = \frac{1}{N_s} \sum_{i=1}^{N_s} \gamma_i \tag{22}$$

where N_s is the number of connections surrounding the solid element. (In this case, $N_s = 8$.)

2.2.1. Use of finite element package for E-ECP models. Because all solid elements should be connected by links for topology optimization, a standard finite element model is difficult to convert to a model suitable for E-ECP. Thus, a systematic conversion technique described in Figure 6 is developed. In Appendix, a Matlab file to convert an ANSYS finite element model to the E-ECP model is presented. An ANSYS file reading the node and element information of the E-ECP model is also presented as ECPMODEL.DAT in APPENDIX.

2.3. Internal ECP (I-ECP): a new development

Although E-ECP is easy to implement even with commercial software, the links introduced to connect solid elements result in a substantial increase of the total degrees of freedom, i.e. the size of the final system matrix. In three-dimensional cases, a connection point is shared by eight solid elements so that the total system matrix size increases by about 8 times than that of the standard density approach. The increased matrix size naturally requires larger memory and more computation time. Therefore, a new ECP-based formulation that does not increase the final system matrix size must be developed to fully overcome this drawback of the ECP method. The new version of the ECP method will be called the internal ECP method (I-ECP) because the connecting links will lie inside discretization pixels or voxels. The main characteristics of I-ECP may be understood if the E-ECP and the I-ECP modelling techniques in Figure 7 are compared.

DOI: 10.1002/nme

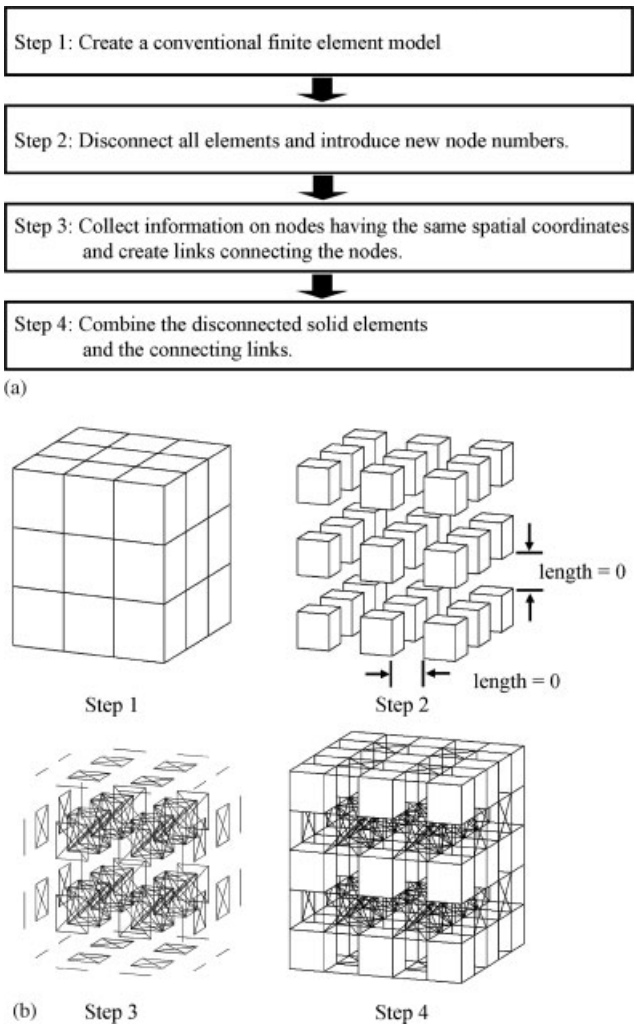

Figure 6. The procedure to convert a standard finite element model to a model needed for the E-ECP method: (a) schematic flow chart; and (b) graphical illustration.

The following is the summary of the essential characteristics of the newly proposed I-ECP method:

(1) All continuum elements used in I-ECP for analysis during topology optimization have the original material properties as in E-ECP.
(2) I-ECP uses zero-length internal links that lie inside every domain-discretizing pixel (or voxel) while E-ECP uses external links that lie outside every pixel (or voxel). In I-ECP, every plane (or solid) element is supported by elastic links at the nodes of its surrounding pixel (or voxel).

DOI: 10.1002/nme

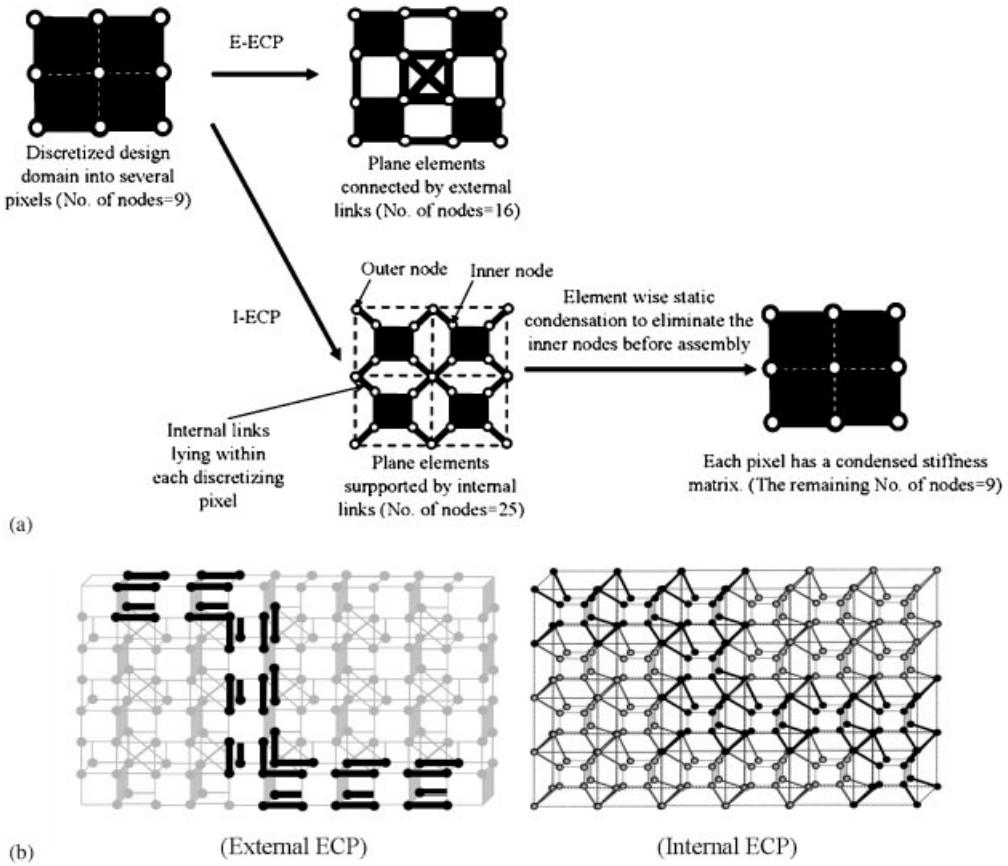

Figure 7. The modelling comparison of the external ECP and the internal ECP: (a) a two-dimensional case; and (b) a three-dimensional case.

(3) Paradoxically, the initial models use more nodes than the E-ECP model for the same discretization resolution, but the degrees of freedom of inner nodes (shown in Figure 7(a)) are condensed out in every pixel (or voxel) level in order to avoid the matrix size increase.
(4) After the condensation, the matrix size of each pixel (or voxel) in I-ECP becomes the same as that of the standard finite element.
(5) The stiffness of all of the internal links lying inside every pixel (or voxel) is controlled by one design variable γ_e.
(6) The density of the eth pixel (or voxel) ρ_e^{raster} is assumed to be proportional to γ_e, i.e.

$$\rho_e^{\text{raster}} = \gamma_e \tag{23}$$

Note that Equation (23) is used only for mass calculation and the rastering of the final optimized result, not for the pixel (voxel) stiffness calculation. To clarify the modelling technique used for I-ECP, Figure 8 is prepared.

DOI: 10.1002/nme

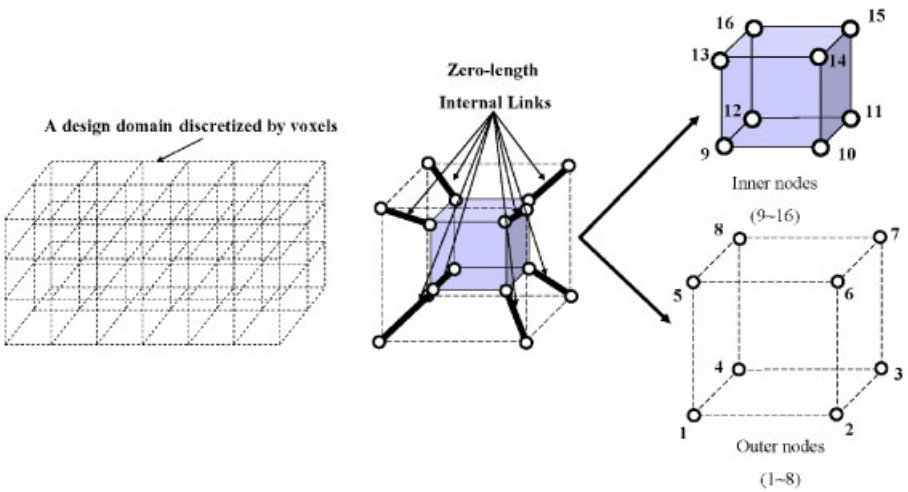

Figure 8. Design domain discretized by voxels. Every voxel contains a solid element. The solid element is connected to the outer nodes that define the edges of a voxel.

2.3.1. Static condensation scheme. The key step to reduce the system matrix size is the static condensation of the inner nodes. This means that only the outer nodes (see Figure 7(a)) connecting discretizing voxels are used for the construction of the system matrix. To explain the static condensation scheme for the geometrically non-linear problem in consideration, let us denote the incremental displacements of the outer and the inner nodes of the eth element at time t of iteration k by $\Delta u^{(k)}_{e,\text{out}}$, and $\Delta u^{(k)}_{e,\text{in}}$, respectively. In the present development, it is assumed that the external force is applied only at the outer nodes. For every voxel, the following incremental equation represents the equilibrium condition:

$$\left\{ \underbrace{\begin{bmatrix} k_{I,e} & -k_{I,e} \\ -k_{I,e} & k_{I,e} \end{bmatrix}}_{\text{Stiffness matrix for links}} + \underbrace{\begin{bmatrix} \mathbf{0} & \mathbf{0} \\ \mathbf{0} & {}^{t}k^{\text{structure},(k-1)}_{\text{T},e} \end{bmatrix}}_{\text{Tangent stiffness matrix for the } e\text{th solid element}} \right\} \underbrace{\begin{bmatrix} \Delta u^{(k)}_{e,\text{out}} \\ \Delta u^{(k)}_{e,\text{in}} \end{bmatrix}}_{\text{The incremental displacement for the } e\text{th voxel}} = \underbrace{\begin{bmatrix} \Re^{(k-1)}_{e,\text{out}} \\ \Re^{(k-1)}_{e,\text{in}} \end{bmatrix}}_{\text{The residual force for the } e\text{th voxel}} \tag{24}$$

where the displacement is updated by the Newton–Raphson scheme as

$$\begin{bmatrix} {}^{t+\Delta t}u^{(k)}_{e,\text{out}} \\ {}^{t+\Delta t}u^{(k)}_{e,\text{in}} \end{bmatrix} = \begin{bmatrix} {}^{t+\Delta t}u^{(k-1)}_{e,\text{out}} \\ {}^{t+\Delta t}u^{(k-1)}_{e,\text{in}} \end{bmatrix} + \begin{bmatrix} \Delta u^{(k)}_{e,\text{out}} \\ \Delta u^{(k)}_{e,\text{in}} \end{bmatrix} \tag{25}$$

In Equation (24), the symbol $\mathbf{0}$ denotes a 24×24 zero matrix for three-dimensional problems. The subscript 'structure' is used to denote the quantities related to the eth solid finite element lying

DOI: 10.1002/nme

inside the eth voxel. The definition of $k_{I,e}$ is

$$k_{I,e} = l_e \mathbf{I}_{24\times 24} \quad \text{(where } \mathbf{I}_{24\times 24} \text{ is a } 24\times 24 \text{ identity matrix)} \tag{26}$$

Simplifying the left-hand side of Equation (24) yields

$$\underbrace{\begin{bmatrix} k_{I,e} & -k_{I,e} \\ -k_{I,e} & k_{I,e} + {}^{t}k_{\mathrm{T},e}^{\mathrm{structure},(k-1)} \end{bmatrix}}_{\substack{\text{The assembled tangent stiffness for} \\ \text{the voxel having the } e\text{th solid element}}} \underbrace{\begin{bmatrix} \Delta u_{e,\mathrm{out}}^{(k)} \\ \Delta u_{e,\mathrm{in}}^{(k)} \end{bmatrix}}_{\substack{\text{The incremental} \\ \text{displacement}}} = \underbrace{\begin{bmatrix} \Re_{e,\mathrm{out}}^{(k-1)} \\ \Re_{e,\mathrm{in}}^{(k-1)} \end{bmatrix}}_{\text{The residual force}} \tag{27}$$

where the residual force terms $\Re_{e,\mathrm{out}}^{(k-1)}$ and $\Re_{e,\mathrm{in}}^{(k-1)}$ for the I-ECP can be found as

$$\begin{bmatrix} \Re_{e,\mathrm{out}}^{(k-1)} \\ \Re_{e,\mathrm{in}}^{(k-1)} \end{bmatrix} = \underbrace{\begin{bmatrix} {}^{t+\Delta t}R_e \\ 0 \end{bmatrix}}_{\text{External Force}} - \underbrace{\begin{bmatrix} 0 \\ {}^{t+\Delta t}_{0}f_e^{\mathrm{structure},(k-1)} \end{bmatrix}}_{\substack{\text{Internal force} \\ \text{from the structure}}} - \underbrace{\begin{bmatrix} {}^{t+\Delta t}_{0}f_{e,\mathrm{out}}^{\mathrm{link},(k-1)} \\ {}^{t+\Delta t}_{0}f_{e,\mathrm{in}}^{\mathrm{link},(k-1)} \end{bmatrix}}_{\substack{\text{Internal force} \\ \text{from the links}}} \tag{28}$$

In Equation (28), ${}^{t+\Delta t}R_e$ and ${}^{t+\Delta t}_{0}f_e^{\mathrm{structure},(k-1)}$ denote the externally applied force on the outer nodes and the internal force acting on the inner nodes, respectively (see also Reference [14]). The internal force terms, ${}^{t+\Delta t}_{0}f_{e,\mathrm{out}}^{\mathrm{link},(k-1)}$ and ${}^{t+\Delta t}_{0}f_{e,\mathrm{in}}^{\mathrm{link},(k-1)}$, can be easily calculated from

$$\begin{bmatrix} {}^{t+\Delta t}_{0}f_{e,\mathrm{out}}^{\mathrm{link},(k-1)} \\ {}^{t+\Delta t}_{0}f_{e,\mathrm{in}}^{\mathrm{link},(k-1)} \end{bmatrix} = \begin{bmatrix} k_{I,e} & -k_{I,e} \\ -k_{I,e} & k_{I,e} \end{bmatrix} \begin{bmatrix} {}^{t+\Delta t}u_{e,\mathrm{out}}^{(k-1)} \\ {}^{t+\Delta t}u_{e,\mathrm{in}}^{(k-1)} \end{bmatrix} \tag{29}$$

The size of the stiffness matrix in Equation (29) for the I-ECP implementation becomes 16×16 for two-dimensional cases and 48×48 for three-dimensional cases.

Since all governing field equations are available, the next step is to condense out the degrees of freedom associated with the inner nodes. Using the second equation of (27), $\Delta u_{e,\mathrm{in}}^{(k)}$ is written as

$$\Delta u_{e,\mathrm{in}}^{(k)} = (k_{I,e} + {}^{t}k_{\mathrm{T},e}^{\mathrm{structure},(k-1)})^{-1}(\Re_{e,\mathrm{in}}^{(k-1)} + k_{I,e}\Delta u_{e,\mathrm{out}}^{(k-1)}) \tag{30}$$

Substituting Equation (30) into the first equation of (27) yields

$$\underbrace{{}^{t}k_{\mathrm{Con},e}^{(k-1)}}_{\substack{\text{The condensed} \\ \text{tangent stiffness matrix} \\ \text{for the } e\text{th voxel}}} \qquad \Delta u_{e,\mathrm{out}}^{(k)} = \underbrace{\Re_{e,\mathrm{out}}^{(k-1)} + k_{I,e}(k_{I,e} + {}^{t}k_{\mathrm{T},e}^{\mathrm{structure},(k-1)})^{-1}\Re_{e,\mathrm{in}}^{(k-1)}}_{\text{The condensed residual force acting on the } e\text{th voxel}} \tag{31}$$

where

$${}^{t}k_{\mathrm{Con},e}^{(k-1)} = (k_{I,e} - k_{I,e}(k_{I,e} + {}^{t+\Delta t}k_{\mathrm{T},e}^{\mathrm{structure},(k-1)})^{-1}k_{I,e}) \tag{32}$$

The condensed tangent stiffness matrix for three-dimensional cases has the dimension of 24×24, which is exactly the same as that for a standard solid element.

DOI: 10.1002/nme

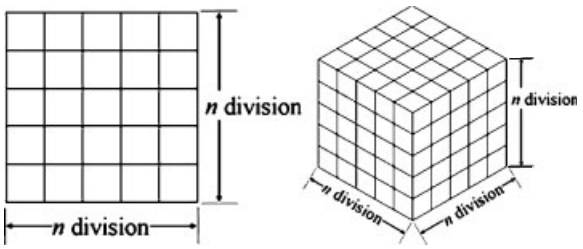

(a)

Methods	Dimension	Total number of nodes introduced	The size of the global system matrix
Element density method	2 D	$(n+1)^2$	$2\times(n+1)^2$
	3 D	$(n+1)^3$	$3\times(n+1)^3$
E-ECP	2 D	$4\times n^2$	$8\times n^2$
	3 D	$8\times n^3$	$24\times n^3$
I-ECP*	2 D	$5\times n^2+2\times n+1$	$2\times(n+1)^2$
	3 D	$9\times n^3+3\times n^2+3\times n+1$	$3\times(n+1)^3$

* The total node number is the sum of the number of internal nodes and the number of external nodes.

(b)

Figure 9. The total node number and the global system matrix size by various approaches: (a) given domain discretization; and (b) comparison.

The global tangent matrix for the whole structural system is now assembled as

$$\underbrace{{}^{t}\mathbf{K}_{\mathrm{Con}}^{(k-1)}}_{\substack{\text{The assembled}\\ \text{condensed tangent}\\ \text{stiffness matrix}}} = \sum_{e=1}^{N_p} {}^{t}k_{\mathrm{Con},e}^{(k-1)} \tag{33}$$

where N_p is the total number of voxels, which is the same as the total number of the solid elements used. The system equation for the assembled global incremental displacement vectors of the outer nodes at iteration k, $\Delta\mathbf{U}_{\mathrm{out}}^{(k)}$, becomes

$$\underbrace{{}^{t}\mathbf{K}_{\mathrm{Con}}^{(k-1)}}_{\substack{\text{The assembled}\\ \text{condensed tangent}\\ \text{stiffness matrix}}} \Delta\mathbf{U}_{\mathrm{out}}^{(k)} = \underbrace{\Re_{\mathrm{Con}}^{(k-1)}}_{\substack{\text{The assembled}\\ \text{condensed residual}\\ \text{force}}} \tag{34}$$

where

$$\Re_{\mathrm{Con}}^{(k-1)} = \sum_{e=1}^{N_d} [\Re_{e,\mathrm{out}}^{(k-1)} + k_{I,e}(k_{I,e} + {}^{t}k_{\mathrm{T},e}^{\mathrm{structure},(k-1)})^{-1}\Re_{e,\mathrm{in}}^{(k-1)}] \tag{35}$$

DOI: 10.1002/nme

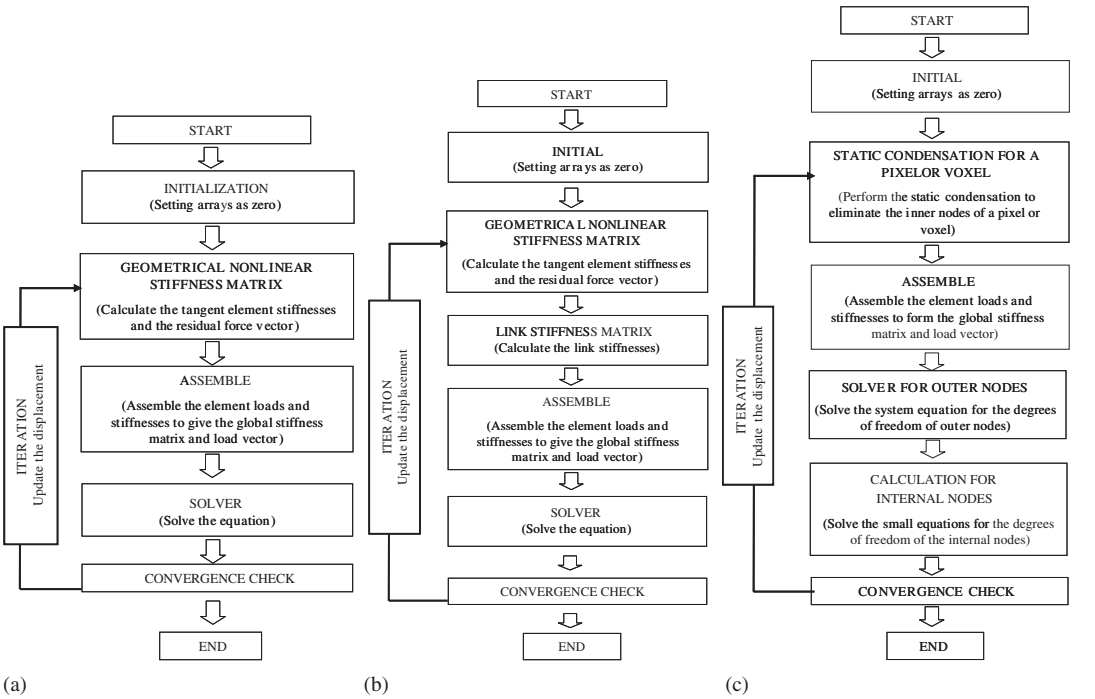

Figure 10. Comparison of the solution procedures of: (a) the standard element density method; (b) the E-ECP method; and (c) the I-ECP method.

After solving for $\Delta\mathbf{U}_{\text{out}}^{(k)}$ by Equation (34), the internal displacement $\Delta u_{e,\text{in}}^{(k)}$ for each voxel can be calculated by Equation (30). Figure 9 compares the total number of nodes used and the global system matrix size for three different approaches. To identify the difference in the three modelling approaches, their analysis procedures are compared in Figure 10. The box 'ITERATION' in Figure 10 implies the iterative procedure of the Newton–Raphson method.

2.4. Numerical stability and efficiency of E-ECP and I-ECP

Before applying the E-ECP and I-ECP methods to topology optimization, both methods will be examined in their numerical performances such as solution accuracy. (Additional discussions on the solution accuracy issue of the E-ECP method may be found in Reference [2].)

First, the effects of the link stiffness value l_e on the solution accuracy and the condition number of the assembled system matrix will be investigated. For this study, a three-dimensional cantilever beam discretized by 10 voxels as shown in Figure 11(a) is selected as an analysis model. The voxels are connected by zero-length links for ECP models while no link is used for a standard finite element model.

Figure 11(b) shows the variation of the vertical displacement δ_{ECP} as l_e/k_{diagonal} varies from 1 to 10^5. The tip displacement by a 10-element standard finite element model is denoted by $\delta_{\text{FEM}} = -518.38$. Both I-ECP and E-ECP yield sufficiently accurate results as l_e/k_{diagonal} be-

DOI: 10.1002/nme

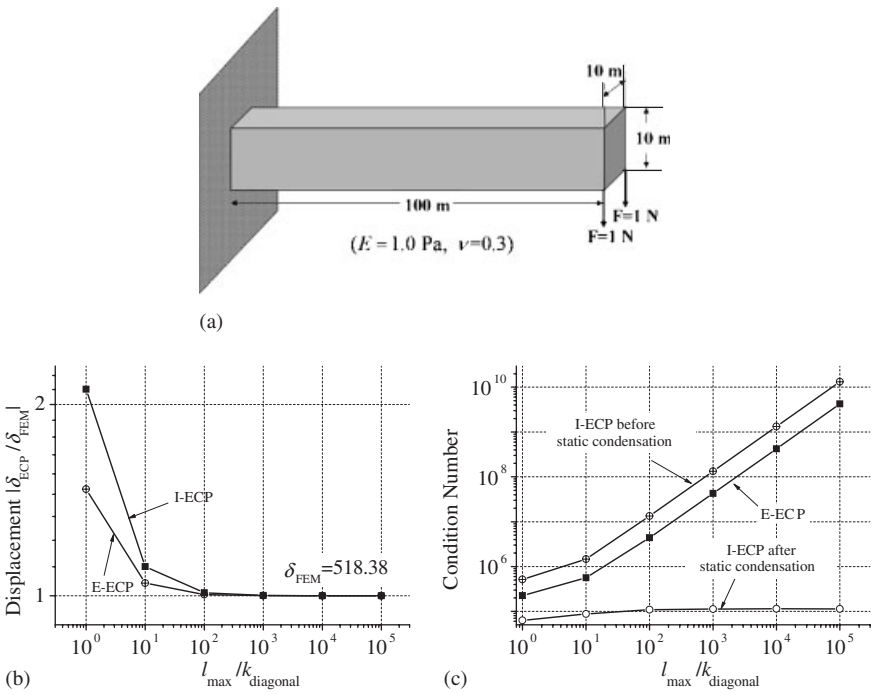

Figure 11. The convergence and the conditions numbers of the ECP methods: (a) the considered linear problem (The standard finite element solution with standard bi-linear brick element provides 518.38 for the displacement (δ_{FEM}) at the tip where the forces are applied.); (b) the displacement convergence with respect to the link stiffness; and (c) the condition numbers of ECP methods. (The diagonal stiffness is denoted by k_{diagonal}.)

comes larger than 10^4 : $\delta_{\text{E-ECP}} = -518.40$, $\delta_{\text{I-ECP}} = -518.44$ for $l_e/k_{\mathrm{diagonal}} = 10^4$, and $\delta_{\text{E-ECP}} = \delta_{\text{I-ECP}} = -518.38$ for $l_e/k_{\mathrm{diagonal}} = 10^5$.

Figure 11(c) shows the condition numbers of the system stiffness matrices for the analysis of the cantilever in Figure 11(a) by the ECP methods. In this figure, the results for the I-ECP method before and after the static condensation are included. When E-ECP and I-ECP$|_{\mathrm{B.C}}$ (the I-ECP before the application of the static condensation) are used, the condition number (which can be calculated as the ratio of the maximum eigenvalue of the system matrix to the minimum eigenvalue) increases as $l_e/k_{\mathrm{diagonal}}$ increases. Because nodes connected by the elastic links introduce additional eigenmodes having the eigenvalues proportional to the link stiffness, the condition number increases. The magnitude of the condition number by E-ECP differs from that of I-ECP$|_{\mathrm{B.C}}$ because the actual system stiffness size is different.

When I-ECP (i.e. I-ECP after the application of the static condensation) is used, the eigenmodes discussed above are eliminated. Consequently, the condition number of the system stiffness matrix of I-ECP approaches that of the stiffness matrix of the standard finite element model as $l_e/k_{\mathrm{diagonal}}$ increases. This limiting behavior is shown in Figure 11(c); the condition number by I-ECP for $l_e/k_{\mathrm{diagonal}} = 10^5$ is 1.13×10^5 and those by a standard finite element model is 1.126×10^5. The

DOI: 10.1002/nme

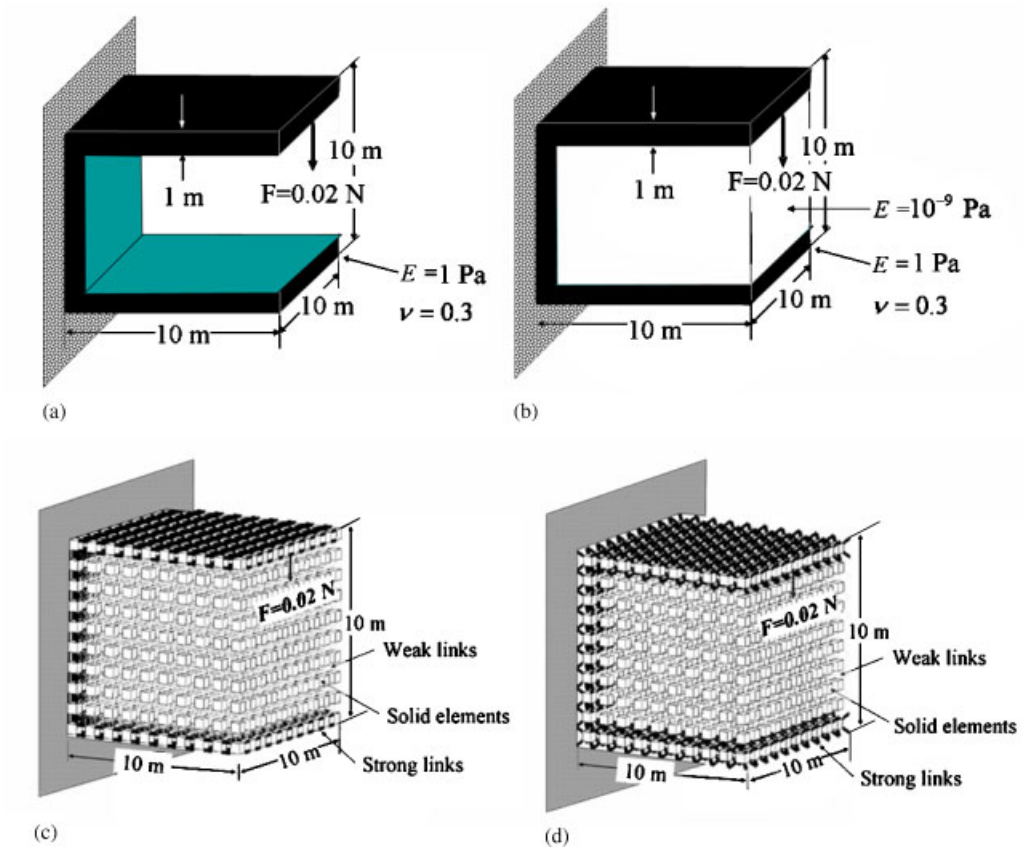

Figure 12. The numerical performance test for a three-dimensional benchmark problem considering geometrical non-linearity: (a) a given model; (b) the model used in the standard element density method; and (c) and (d) the models used in the E-ECP method and the I-ECP method, respectively (F: applied force, E: Young's modulus).

small condition number by I-ECP (after the static condensation) is also very useful especially when an iterative solver is used.

Now, the solution convergence of the Newton–Raphson method and the computation time for non-linear problems will be studied. The problem depicted in Figure 12(a) is solved by the element density method, E-ECP, and I-ECP. The numerical performances of the three methods are compared in Figure 13. The direct finite element approach using the model in Figure 12(a) and the E-ECP/I-ECP methods yielded the identical tip displacement up to the three decimal points (the vertical displacement: -3.679) as shown in Table I. If the L_2-norm of the incremental residual $\Re^{(k)}$ in the Newton–Raphson method becomes equal to or less than 10^{-6}, the corresponding solution is considered the converged solution. To facilitate the comparison of the numerical performances for the benchmark problem shown in Figure 12, the Crout factorization method with the

DOI: 10.1002/nme

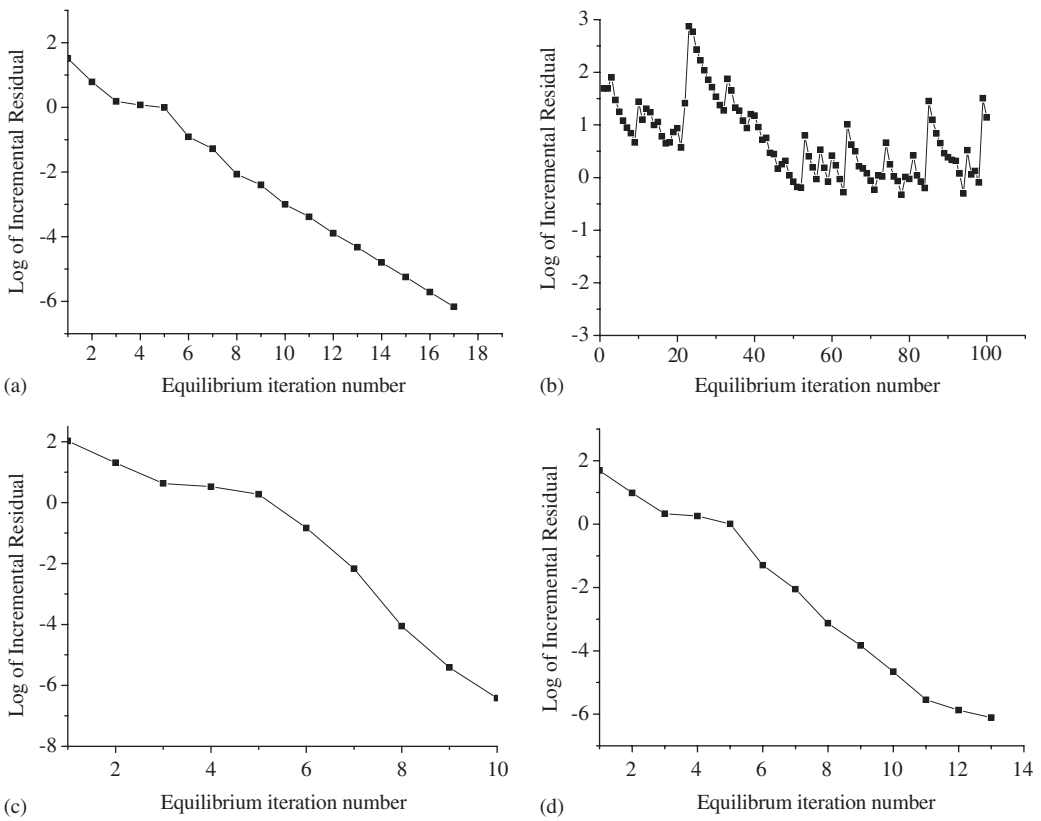

Figure 13. The history of the incremental residual $\Re^{(k)}$ in the Newton–Raphson method based on: (a) the original model; (b) the model by the element density method; and (c), (d) the models by the E-ECP and I-ECP methods for the problem shown in Figure 12.

bandwidth reduction algorithm (TOMS 508 in the Netlib library [16]) is used.[‖] A Pentium computer (2.59 GHz XEON CPU, 4 GB RAM) was used for the comparison.

From the results in Figure 13 and Table I, the following conclusions may be drawn:

(1) Both E-ECP and I-ECP yield stably converging results, unlike the element density method.
(2) The solution accuracy by the ECP method is similar to that by direct analysis using the model in Figure 12(a).

[‖]For topology optimization problems considered in the next section, the preconditioned conjugate gradient (PCG) method is used to reduce the required computer memory size. For instance, the second example in the next section required less than 60 MB RAM for the PCG method whereas over 2 GB RAM, causing an overflow error on a 32 bit operating system, was required for the direct solver using the LU decomposition. However, since several parameters of the PCG solver varied depending on the topology optimization modelling methods, we used the standard direct solver to solve the benchmark problem in this section for accurate comparison of different topology optimization modelling techniques. Nevertheless, the numerical findings with the direct solver were almost the same to those with the PCG solvers.

DOI: 10.1002/nme

Table I. The comparison of the total CPU time and the number of iterations for the benchmark problem shown in Figure 12.

Method	Direct analysis using the model in Figure 12(a)	Density method	E-ECP method	I-ECP method
Displacement at the loaded point	(0.000, −1.206, −3.679)	No convergence	(0.000, −1.206, −3.679)	(0.000, −1.206, −3.679)
Number of the Newton–Raphson iterations	16	No convergence	10	14
Total CPU time (s)	74.7	No convergence	1488.4	200.5

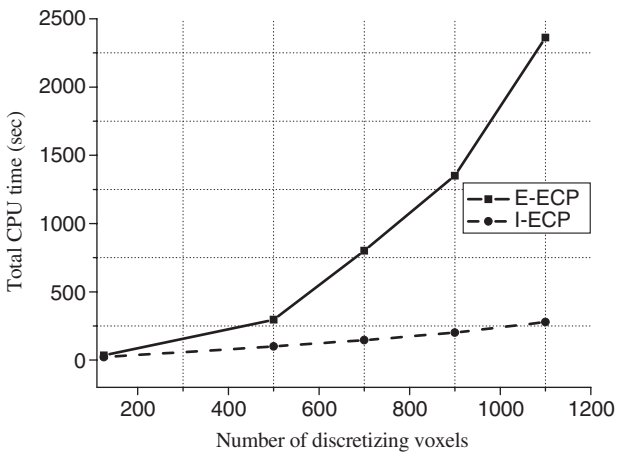

Figure 14. Comparison of the numerical efficiencies of E-ECP and I-ECP methods using non-linear analysis at various discretization levels of the problem defined in Figure 11(a).

(3) The I-ECP method yields less computation time than the E-ECP method because the system matrix size is reduced by the static condensation of the inner nodes.

To show the advantage of the I-ECP method over the E-ECP method in terms of computational efficiency, the geometrically non-linear analysis of a three-dimensional cantilever structure subjected to an end couple shown in Figure 11(a) is also considered. The total CPU times of both methods at various discretization levels are compared in Figure 14. For fair comparison, the accumulated CPU time spent for the first twenty Newton–Raphson iterations was compared between the two methods. Figure 14 clearly shows that I-ECP with the static condensation scheme yields significantly less CPU time than E-ECP, especially at high discretization levels.

DOI: 10.1002/nme

3. TOPOLOGY OPTIMIZATION BY E-ECP AND I-ECP

Since the stability of the two ECP methods for numerical analysis has been demonstrated in the previous section, the effectiveness of the ECP methods in the topology optimization of three-dimensional geometrically non-linear problems will be investigated in this section. The underlying optimization formulation of the ECP method is outlined below. If the formulation given in Reference [1] for E-ECP is slightly modified, it can be directly applied for I-ECP; thus no detailed optimization formulation for I-ECP will be given here. Three-dimensional compliance minimization problems will be considered to check the performances of the E-ECP and I-ECP methods. The optimality criteria (OC) method was used as the optimization algorithm [4].

The topology optimization for the compliance minimization of geometrically non-linear structures can be written as

$$\underset{\boldsymbol{\gamma}}{\text{Minimize}} \quad W(\boldsymbol{\gamma}) = \mathbf{L}^{\mathrm{T}\,t+\Delta t}\mathbf{U}(\boldsymbol{\gamma}) \tag{36}$$

$$\text{Subject to} \quad H = \sum_{e=1}^{N_p} \rho_e(\boldsymbol{\gamma}) V_e - V^* \leqslant 0 \tag{37}$$

where the equilibrium condition (8) is assumed to be satisfied in the form of either (15) or (34). The equilibrium state is assumed to be reached at time $t+\Delta t$ for a given load. In Equation (36), $\mathbf{L}$ is the load vector consisting of zeros except for the positions where loads are applied, and ${}^{t+\Delta t}\mathbf{U}$ denotes the converged displacement of the geometrically non-linear analysis.

To facilitate the sensitivity calculation of $\mathrm{d}W/\mathrm{d}\gamma_i$, it is convenient to use the adjoint variables ${}^{t+\Delta t}\boldsymbol{\lambda}$ which satisfy

$${}^{t+\Delta t}\mathbf{K}_{\mathrm{T}}{}^{t+\Delta t}\boldsymbol{\lambda} = \mathbf{L} \tag{38}$$

where ${}^{t+\Delta t}\mathbf{K}_{\mathrm{T}}$ is the tangent stiffness matrix for the converged state of equation $t+\Delta t$ of the geometrically non-linear analysis. The definition of ${}^{t+\Delta t}\mathbf{K}_{\mathrm{T}}$ is given in Equation (18) for E-ECP and in Equation (33) for I-ECP. Following the procedure given in Reference [1], one can show that the sensitivity $\mathrm{d}W/\mathrm{d}\gamma_i$ becomes

$$\frac{\mathrm{d}W}{\mathrm{d}\gamma_i} = -\,{}^{t+\Delta t}\lambda_i^{\mathrm{T}} \frac{\mathrm{d}k_i^{\mathrm{link}}}{\mathrm{d}\gamma_i}\,{}^{t+\Delta t}u_i \tag{39}$$

where ${}^{t+\Delta t}\lambda_i$ and ${}^{t+\Delta t}u_i$ are the adjoint variable vector and the converged displacement vector defined on the link set at the ith connection.

3.1. Case study 1: compliance minimization of a structure with all side surfaces fixed

As the first numerical example, the compliance minimization of the structure shown in Figure 15(a) is considered (mass constraint ratio = 20%). A downward force of $F = 6.9 \times 10^7$ N is applied at the center of the top surface. The side surfaces are all clamped. The three results in Figure 15(b) are those obtained by the density method using *linear* analysis, the E-ECP method using *non-linear* analysis, and the I-ECP method using *non-linear* analysis, respectively. It was difficult to obtain a converged solution by the element density method without some numerical treatments for non-linear analysis. Thus, only the linear result is presented. Almost identical layout configurations were obtained by E-ECP and I-ECP.

DOI: 10.1002/nme

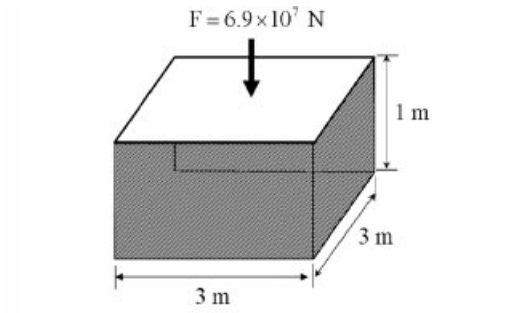

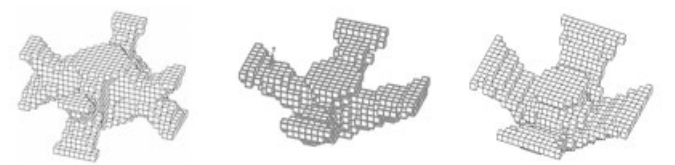

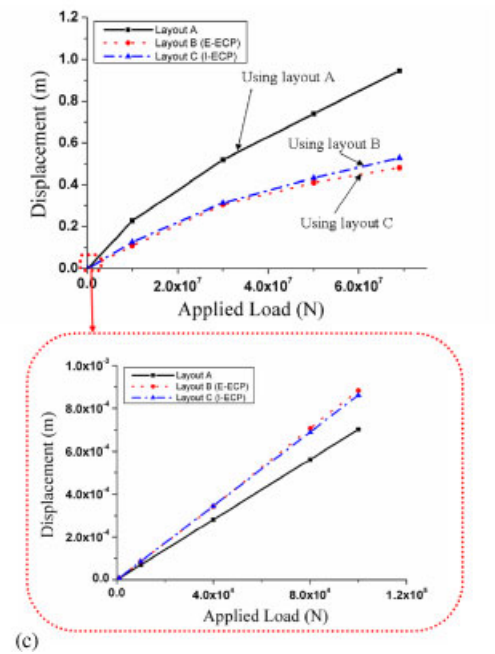

Figure 15. Compliance minimization of a structure with all side surfaces fixed: (a) problem definition (the design domain is descretized by $30 \times 30 \times 10$ voxels); (b) optimized layouts; and (c) the load–deflection curve obtained at the loaded point.

DOI: 10.1002/nme

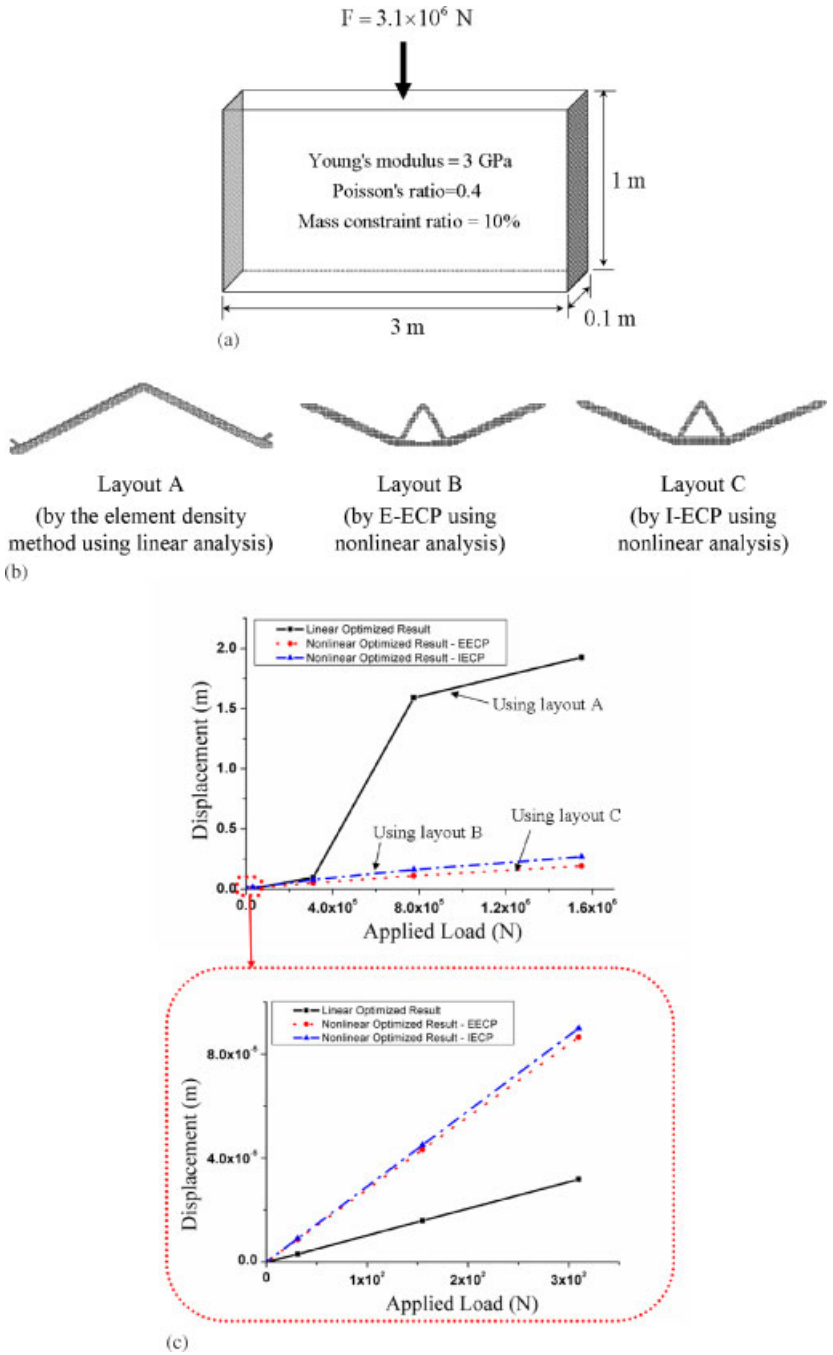

Figure 16. Compliance minimization of a slender body with its two side surfaces fixed: (a) problem definition (the design domain is discretized by $120 \times 40 \times 2$ voxels); (b) optimized layouts; and (c) the load–deflection curve obtained at the loaded point.

DOI: 10.1002/nme

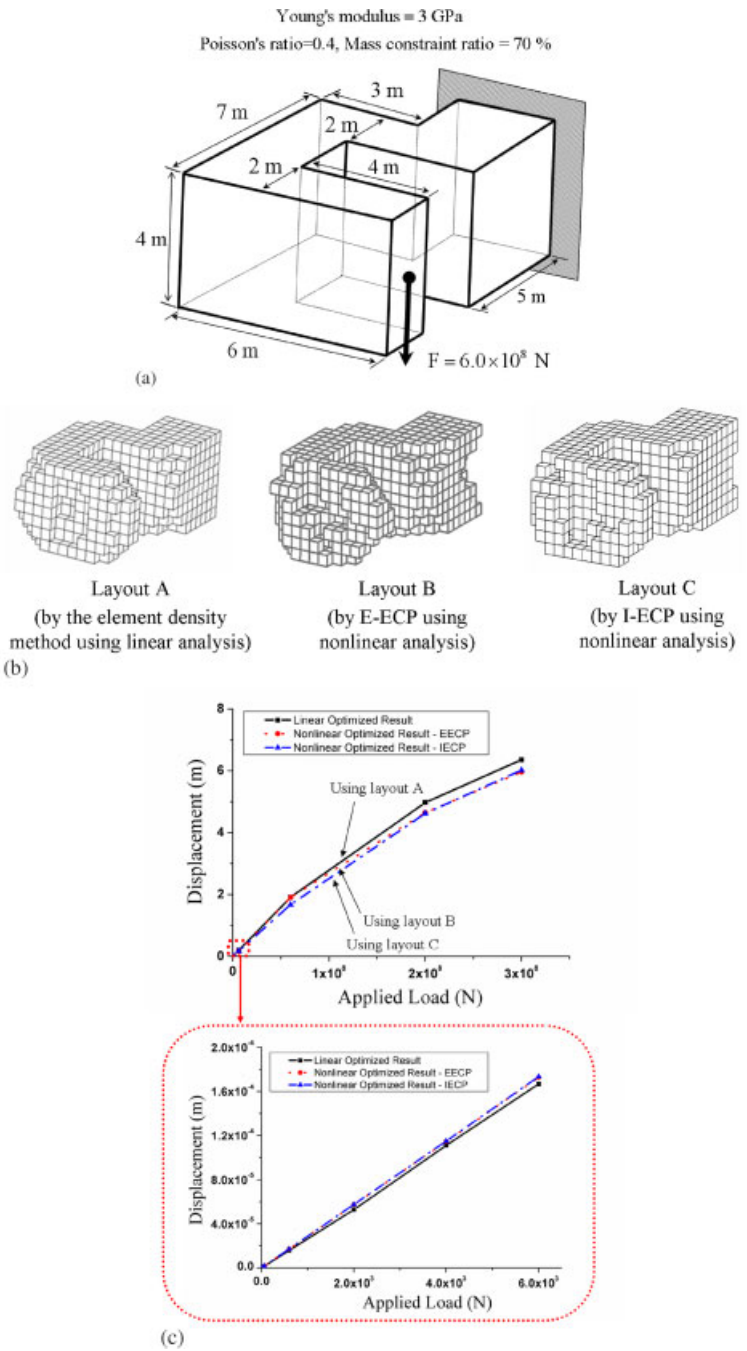

Figure 17. Compliance minimization of a hook structure with one side fixed: (a) problem definition (The design domain is discretized by 1248 voxels.); (b) optimized layouts; and (c) the load–deflection curve obtained at the loaded point.

DOI: 10.1002/nme

Using the topological layouts in Figure 15(b), the load–deflection relations at the loaded point are compared in Figure 15(c). Figure 15(c) shows that geometrical non-linearity is important to consider when the applied force is large. As expected, the optimized result by the linear analysis performs better than those by the non-linear analysis for a small load. The slight difference between the force-displacement curves by two ECP methods in Figure 15(c) appears to result from the different numerical characteristics of the two methods as evidenced by Figures 11(b) and (c) and Figures 13(c) and (d) and the presence of many local optima.

3.2. Case study 2: compliance minimization of a slender body with two sides fixed

As the second case study, a slender body shown in Figure 16(a) is considered. The optimized results by three different approaches are shown in Figure 16(b). To obtain the results, the layout symmetry was used. The results obtained by the ECP methods for this three-dimensional problem are similar to those obtained for the two-dimensional cases [1, 6, 7]. The optimal layout by E-ECP is almost the same as that of I-ECP. The load–deflection curve at the loaded tip is plotted in Figure 16(c). Obviously, Layout A performs better when the applied load is small but will experience a snap-through when the applied load exceeds a certain value. The optimal topologies by two ECP methods are also almost the same. The load–displacement relations for the two results obtained by E-ECP and I-ECP are very close although they are not exactly the same.

3.3. Case study 3: compliance minimization of a hook structure

As the last example, the compliance minimization of a hook structure shown in Figure 17(a) is considered to demonstrate the applicability of the ECP methods to problems defined on arbitrarily-shaped design domains. The optimized results are shown in Figure 17(b), and the load–deflection curve is shown in Figure 17(c). Since there is no phenomenon such as a snap-through, the stiffness increases of Layouts B and C obtained by non-linear analysis are not so significant. However, this example demonstrates that the developed ECP methods including the I-ECP method can be applied to arbitrarily-shaped domains.

4. CONCLUSIONS

In this paper, the topology optimization of three-dimensional geometrically non-linear structures was carried out by two versions of the element connectivity parameterization (ECP) methods, the external ECP (E-ECP) method and the internal ECP (I-ECP) method. Unlike the element density method, both methods yield numerically stable results because the solid finite elements used to predict the structural response of a three-dimensional body remained solid throughout the optimization of the ECP methods. When the newly-developed I-ECP was used, zero-length links controlling inter-element connectivity were placed within each of the domain-discretizing voxels. The element wise static condensation of inner nodes enhanced the computational efficiency of I-ECP considerably. The E-ECP method, which directly connects the nodes of solid voxels, required more computation time than I-ECP, but could directly incorporate commercial analysis software for the analytic sensitivity calculation needed for topology optimization.

DOI: 10.1002/nme

APPENDIX

A Matlab file, called CONVERT.M, converts a standard finite element model generated by ANSYS to a model needed for the E-ECP method. The generated files by CONVERT.M are 'ecp.nod' (node information) and 'ecp.ele' (element information).

CONVERT.M

```
% Read in properly formatted data files of a finite element model by ANSYS 6.0
% node.dat and element.dat contain node and element information
load node.dat; load element.dat;
% Set the default parameters
epi=1.0E-6; en=1;
nformat='%8d%20.13f%20.13f%20.13f\r\n';
eformat='%6d%6d%6d%6d%6d%6d%6d%6d%6d%6d%6d%6d%6d%6d%6d\r\n';

% Node information generation for the E-ECP method
fid=fopen('ecp.nod','w');
for k=1:size(element,1),
  fprintf(fid,nformat,[8*k+[-7:0]; node(element(k,1:8),2:4)']);
end
fclose(fid);

% Link element information generation for the E-ECP method
load ecp.nod
fid=fopen('ecp.ele','w');
% For link elements
for k=1:size(element,1)*8;
  for l=k+1:size(element,1)*8;
   if norm([ecp(k,2:4)-ecp(l,2:4)]) <epi
   fprintf(fid,eformat,[ecp(k,1),ecp(l,1),zeros(6,1)', [1 2 1 1 0,en]]);en=en+1;
   end
  end
end

% Disconnected solid element information generation for the E-ECP method
for k=1:size(element,1),
  fprintf(fid,eformat,[[k*8-7:1:k*8],ones(1,4),0,en]); en=en+1;
end
fclose(fid);
```

ECPMODEL.DAT

```
/prep7
LENUM=(User define)      ! Set the number of links
Et,1,45                  ! Solid element
Et,2,27                  ! Link element
KEYOPT,2,3,4
nread,ecp,nod            !Read the node information
```


DOI: 10.1002/nme

```
 7. eread,ecp,ele                !Read the element information

 8. MP,EX,1,(User define)        ! Young's modulus
 9. MP,NUXY,1, (User define)     ! Poisson's ratio
10. MaxLinkE=(User define)       ! Set the maximum link stiffness
11. MinLinkE=(User define)       ! Set the minimum link stiffness
12. N=(User define)              ! Penalization parameter
13. M=(User define)              ! Penalization parameter
14. AL=MaxLinkE-MinLinkE         ! Auxiliary parameter
15. BE=MinLinkE                  ! Auxiliary parameter

16. *do,i,1,LENUM,1              ! Update the link stiffness
17. ECH=AL* (dv(i))**N)/(1+(1-dv(i)**N)*M)+BE
18. R,i
19. RMODIF,i,1,ECH
20. RMODIF,i,13,ECH
21. RMODIF,i,24,ECH
22. RMODIF,i,7,-ECH
23. RMODIF,i,19,-ECH
24. RMODIF,i,30,-ECH
25. RMODIF,i,58,ECH
26. RMODIF,i,64,ECH
27. RMODIF,i,69,ECH
28. EMODIF,i,REAL,i,
29. *enddo

30. ! Apply the boundary condition and solve
31. ! Calculate the sensitivity analysis
```

ACKNOWLEDGEMENTS

This work is supported by the National Creative Research Initiatives Program (Korea Science Foundation Grant) contracted through the Institute of Advanced Machinery and Design at Seoul National University.

REFERENCES

1. Yoon GH, Kim YY. Element connectivity parameterization for topology optimization of geometrically nonlinear structures. *International Journal of Solids and Structures* 2005; **42**(7):1983–2009.
2. Yoon GH, Kim YY. The element connectivity parameterization for the topology design optimization of multiphysics systems. *International Journal for Numerical Methods in Engineering* 2005; **64**:1649–1677.
3. Bendsøe MP, Kikuchi N. Generating optimal topologies in structural design using a homogenization method. *Computer Methods in Applied Mechanics and Engineering* 1988; **71**:197–224.
4. Bendsøe MP, Sigmund O. *Topology Optimization Theory*, *Methods and Applications*. Springer: New York, 2003.
5. Jung DY, Gea HC. Topology optimization of nonlinear structures. *Finite Elements in Analysis and Design* 2004; **40**(11):1417–1427.
6. Bruns TE, Tortorelli DA. An element removal and reintroduction strategy for the topology optimization of structures and compliant mechanisms. *International Journal for Numerical Methods in Engineering* 2003; **57**:1413–1430.

DOI: 10.1002/nme

7. Buhl T, Petersen CBW, Sigmund O. Stiffness design of geometrically nonlinear structures using topology optimization. *Structural and Multidisciplinary Optimization* 2000; **19**(2):93–104.
8. Cho SH, Jung HS. Design sensitivity analysis and topology optimization of displacement-loaded nonlinear structures. *Computer Methods in Applied Mechanics and Engineering* 2003; **192**:2539–2553.
9. Cho SH, Jung HS. Reliability-based topology optimization of geometrically nonlinear structures with loading and material uncertainties. *Finite Elements in Analysis and Design* 2004; **43**(7):311–331.
10. Folgado J, Fernandes PR, Rodrigues H. Topology optimization of three-dimensional structures under contact conditions. *Published in WCSMO-4*; *Forth World Congress on Structural and Multidisciplinary Optimization*, Dalian, China, 2001.
11. Chiandussi G, Gaviglio I, Ibba A. Topology optimization of an automotive component without final volume constraint specification. *Advanced in Engineering Software* 2004; **35**(10–11):609–617.
12. Zienkiewicz OC, Talyor RL, Sherwin SJ, Piero J. On discontinuous Galerkin methods. *International Journal for Numerical Methods in Engineering* 2003; **58**:1119–1148.
13. Bruns TE. Topology optimization by penalty method (TOP). *Published in WCSMO-6*; *Sixth World Congress on Structural and Multidisciplinary Optimization*, Rio de Janeiro, Brazil, 2005.
14. Bathe KJ. *Finite Element Procedures*. Prentice-Hall: Englewood Cliffs, NJ, 1996.
15. Yoon GH, Langelaar M, Kim YY, Keulen FV. Stiffness of the elastically supported patch of the internal ECP method and penalization of design variables of internal links for topology optimization, under preparation.
16. TOMS library in www.netlib.org.

DOI: 10.1002/nme